TESTING OF TURBULENT SEALS FOR ROTORDYNAMIC COEFFICIENTS

Dara W. Childs
Department of Mechanical Engineering
Texas A&M University
College Station, Texas 77843

John B. Dressman
Department of Mechanical Engineering
The University of Louisville
Louisville, Kentucky 40208

SUMMARY

A facility has been developed for dynamic testing of straight and convergent-tapered seals with the capability of measuring the radial and tangential force components which result from a circular centered orbit. The test apparatus causes the seal journal to execute small-eccentricity centered circular orbits within its clearance circle. Dynamic measurements are made and recorded of the seal-displacement-vector components, and of the pressure field. The pressure field is integrated to yield seal tangential and radial reaction-force components. Representative test data are provided and discussed for straight seals.

NOMENCLATURE

A	: amplitude of orbital motion (L)
C_r	: radial clearance (L)
$\tilde{C}$, $\tilde{c}$	: nondimensional, direct and cross-coupled damping coefficients, introduced in Eq. (4)
C, c	: direct and cross-coupled damping coefficients, introduced in Eq. (6), (FT/L)
H	: clearance function (L)
$\tilde{K}$, $\tilde{k}$	: nondimensional, direct and cross-coupled stiffness coefficients, introduced in Eq. (4)
K, k	: direct and cross-coupled stiffness coefficients, introduced in Eq. (6), (F/L)
L	: seal length (L)
$\tilde{M}$, $\tilde{m}$	: nondimensional, direct and cross-coupled added-mass coefficients, introduced in Eq. (4)
M, m	: direct and cross-coupled added mass coefficients introduced in Eq. (6), (M)

*The work reported herein was supported by NASA Lewis under NASA Grant 3200; technical monitor, Dr. Robert C. Hendricks.

ΔP : seal differential pressure, (F/L^2)

r_X, r_Y : components of seal-displacement vector, introduced in Eq. (4), (L)

R_X, R_Y : component of seal reaction force, introduced in Eq. (4), (F)

R : seal radius, (L)

$R_a = 2VC/\nu$: nominal, leal axial Reynolds number

$R_c = R\omega C/\nu$: nominal, seal circumferential Reynolds number

$T = L/V$: transit time of fluid through seal, (T)

V : nominal flow velocity of fluid through seal, (L/T)

λ : friction factor, defined in Eq. (3)

ν : fluid kinematic viscosity, (L^2/T)

ξ : entrance loss factor, introduced in Eq. (1)

σ : friction loss factor defined in Eq. (2)

ρ : fluid density (M/L^3)

ω : shaft angular velocity (T^{-1})

INTRODUCTION

Black [1,2,3,4], in a series of publications incorporating theoretical and experimental results, has demonstrated that the rotordynamic behavior of pumps is critically dependent on forces developed by neck-rings and interstage seals illustrated in Figure 1. Subsequent experience [5] has demonstrated that the stability of cryogenic turbopumps is comparably dependent on seal forces. The test program discussed here was stimulated by stability difficulties encountered in developing the turbopump of [5], and has the objective of measuring radial and tangential force components for straight and convergent-tapered seals over a range of axial and circumferential Reynolds numbers.

Seal Analysis: Leakage and Dynamic Coefficients

Black [1,2,3,4] is largely responsible for developing models for constant clearance seals. Black's analysis yields a definition of the force acting on a rotor due to its motion at a seal location, and is based on the following leakage relationship from Yamada [6] for flow between concentric rotating cylinders:

$$\Delta P = (1 + \xi + 2\sigma)\rho V^2/2 \qquad (1)$$

where ξ is a constant entry-loss coefficient, ρ is the fluid density, V is the average fluid velocity, and σ is a friction-loss coefficient defined by

$$\sigma = \lambda L/C_r \quad . \tag{2}$$

In the above, L is the seal length, C_r is the radial clearance, and λ has been defined by Yamada to be the following function of the axial and circumferential Reynolds numbers (R_a , R_c)

$$\lambda = 0.079\, R_a^{-1/4}\left[1+ \left(\frac{7R_c}{8R_a}\right)^2\right]^{3/8} \quad , \; R_a = 2VC_r/\nu, \; R_c = R\omega C_r/\nu, \tag{3}$$

where ν is the fluid's kinematic viscosity, R is the seal radius, and ω is the rotor's rotational speed. The friction law definition of Eq. (3), Yamada's definition for λ, is based on an assumed 1/7 power velocity distribution, and fits the Blasius equation for pipe friction.

From a rotordynamic viewpoint, the objective of seal analysis is the definition of seal force coefficients, i.e., stiffness, damping, and added mass terms. In nondimensional form, the force/motion relationship for a seal may be stated

$$-\frac{\lambda}{\pi R\Delta P}\begin{Bmatrix} R_X \\ R_Y \end{Bmatrix} = \begin{bmatrix} \tilde{K} & \tilde{k} \\ -\tilde{k} & \tilde{K} \end{bmatrix}\begin{Bmatrix} r_X \\ r_Y \end{Bmatrix} + T\begin{bmatrix} \tilde{C} & \tilde{c} \\ -\tilde{c} & \tilde{C} \end{bmatrix}\begin{Bmatrix} \dot{r}_X \\ \dot{r}_Y \end{Bmatrix} + T^2\begin{bmatrix} \tilde{M} & \tilde{m} \\ -\tilde{m} & \tilde{M} \end{bmatrix}\begin{Bmatrix} \ddot{r}_X \\ \ddot{r}_Y \end{Bmatrix} \tag{4}$$

where ($\tilde{K}$, $\tilde{C}$, $\tilde{M}$) and ($\tilde{k}$, $\tilde{c}$, $\tilde{m}$) are, respectively, the direct and cross-coupled stiffness, damping, and added-mass terms.

Prior Analytical Results for Constant-Clearance Seals

Test results for the constant-clearance geometry seals are presented and discussed here. Comparable results for convergent-tapered seal geometries will be presented subsequently. The contents of this section are provided to briefly review theoretical and experimental results and procedures for this seal configuration.

Seal analyses which have been published to-date use bulk-flow models in which the raial variation of the velocity and pressure fields across the fluid film are neglected. Governing equations consist of axial and circumferential momentum equations, and the continuity equation for the axial and circumferential velocity components, $U_Z(Z,\theta)$,$U_\theta(Z,\theta)$,$p(Z,\theta)$, which are averaged with respect to the radial coordinate, r. Most reported analyses of seals use a perturbation analysis in the eccentricity ratio of the form

$$H = H_0 + \varepsilon H_1, U_\theta = U_{\theta 0} + \varepsilon U_{\theta 1}$$
$$U_Z = U_{Z0} + \varepsilon U_{Z1}, \; p = p_0 + \varepsilon p_1 \tag{5}$$

where H is the clearance function, and ε is the eccentricity ratio. Governing equations for p_0, $U_{\theta 0}$, U_{Z0} define the centered, zero-eccentricity flow field, while the first-order equations for the variables $U_{\theta 1}$, U_{Z1}, p_1 define the flow fields which result from small motion about a centered position defined by the clearance function $H_1(t,\theta)$. A "short-seal" solution results if $U_{\theta 1}$, "the pressure-induced circumferential flow, " is assumed to be negligible in comparison to the shear-induced term $U_{\theta 0}$. Black [1] initially developed an analytic short-seal solution,

but then with Jensen [2] developed a numerical finite-length solution. Correction factors were developed by Black and Jensen from the finite-length solution to be used in adjusting the short-seal solution to account for finite L/D ratios. Black's second refinement of the original theory was to account for the influence of a change in clearance on local Reynolds numbers [3].

Finally, Black et al. [4] examined the influence of inlet swirl on seal coefficients. In previous analyses, a fluid element entering a seal was assumed to instantaneously achieve the half-speed tangential velocity, $U_\theta = R\omega/2$. The results in [4] demonstrate that a fluid element may travel a substantial distance along the seal before asymptotically approaching this limiting velocity. For interstage seals in which the inlet tangential velocity is negligible, the practical consequences of accounting for this "swirl" effect is a marked reduction in predictions for the cross-coupled stiffness coefficient, k. Black's experimental results show clear evidence of the influence of swirl. A short-seal analysis is used in [4], and the perturbation in Reynolds number due to a local change in clearnace introduced in [3] is not included.

One of the authors [7,8] has recently completed two analyses based on Hirs' turbulent lubrication model [9]. Short and finite-length solutions are developed in [7] and [8], respectively, including all of the various influences introduced in Black's initial analyses [1-4]. The results resemble, but do not coincide with, Black's.

Prior Seal Testing Procedures and Results

The pertinent data which must be measured to confirm the seal leakage model of Eqs. (1) through (3) are ΔP, V,(from flow rate), ω, and the axial pressure gradient within the seal. This latter measurement yields σ which in turn yields λ. Yamada's model for the friction factor was based on testing for these variables over the Reynolds number range ($200 \leq R_a \leq 40{,}000$; $0 \leq R_c \leq 40{,}000$) and clearance to radius ratios of ($.0106 \leq C_r/R \leq .0129$).

Various approaches can be taken to the measurement of rotordynamic coefficients of Eq. (4). For example, if the journal segment of the seal is stationary (i.e., $r_X = r_Y = \dot{r}_X = \dot{r}_Y = 0$), Eq. (4) can be inverted to obtain

$$\begin{Bmatrix} r_X \\ r_Y \end{Bmatrix} = \frac{\lambda}{R\rho\Delta P K_e^{\,2}} \begin{bmatrix} \tilde{K} & -\tilde{k} \\ \tilde{k} & \tilde{K} \end{bmatrix} \begin{Bmatrix} R_X \\ R_Y \end{Bmatrix} , \quad \tilde{K}_e^{\,2} = \tilde{K}^2 + \tilde{k}^2 .$$

Hence, by applying the static load definition ($F_X = F_s$, $F_Y = 0$), and measuring the displacement components, r_X and r_Y, one obtains a combined measure of the direct and cross-coupled stiffness coefficients. This is predominantly the type of testing performed by Black, who cites results in the form of "receptance magnitudes," i.e.,

$$|r|/F_s = \lambda\{\tilde{K}^2 + \tilde{k}^2\}^{\frac{1}{2}}/R\Delta P .$$

The relative magnitudes of the direct $\tilde{K}$ and cross-coupled $\tilde{k}$ stiffness coefficients depend on the relative magnitudes of the axial and radial Reynolds numbers.

Specifically, at zero running speeds, $\tilde{k}$ is zero, but increases with R_c and can exceed K.

Most of Black's testing [2,3,10,11] has been of the static nature cited above. The second type of test cited consists of analytically modelling a test rotor including the theoretically predicted seal dynamics, and comparing the dynamic characteristics of the model with test data. For example, in [2], the test rotor was rapped and a correlation was made with the observed logarithmic decrement on the decay curve. In [3], known imbalances were applied to the test rotor, and a comparison was made with synchronous amplitudes and phase, critical speed location, and onset speed of instability. Comparisons between rotor model results and tests, of this nature, are helpful in deciding whether the general seal model is reasonable. However, this type of test-correlation yields limited specific information about the individual dynamic coefficients. Further, discrepancies in synchronous amplitude and phase results could result from an inadequate initial balance.

A summary of the test results of references [2,3,10,11] is provided in Table 1. The correlation in these tests ranges from "good" to "fair." The nature and results of the test support the following general conclusions concerning the adequacy of Black's dynamic seal model:

(a) Over the Reynolds number range tested, the prediction of the direct stiffness coefficient K is adequate for plain and serrated seals, although less accurate for serrated seals. Black's test results indicate a divergence between tests and theory for the direct damping coefficient C as the axial Reynolds number is increased.

(b) Although the data cited generally supports Black's dynamic seal model over the Reynolds number range considered, it is inadequate to specifically verify the proposed relationships [Eq. (4)] for the dynamic coefficients as functions of the axial and radial Reynolds numbers.

THE UNIVERSITY OF LOUISVILLE DYNAMIC SEAL TEST PROGRAM

Test Section Design

Figure 2 illustrates the test-section design employed in the current seal test program. Water enters the center of the section and flows axially across the two rotating test seals exiting at the bottom of the test section. The seal journals (L = 4 in = 10.16 cm, D = 2 in = 5.08 cm) are mounted eccentrically on the shaft with a constant eccentricity, A = .005 in = 1.27×10^{-4} m. The nominal seal clearance is C_r = .020 in = 5.08 mm, which yields C_r/R = .010. Accordingly, shaft rotation causes the seal journals to execute circular centered orbits at the nominal eccentricity ratio $\varepsilon = 0.25$. Axial and circumferential Reynolds numbers may be specified over the range $R_a \varepsilon [5{,}000, 30{,}000]$, $R_c \varepsilon [0, 11{,}000]$ by varying the shaft rotational speed (0-4,000 rpm) and flowrate. Shaft-speed is measured by a once-per-revolution counter, while turbine flowmeters separately measure flowrate through each seal.

The rotor of Figure 2 is supported in Torrington hollow roller bearings[1] [12]. These precision bearings are preloaded radially, have zero internal clearances, and an accurately predictable radial stiffness. The first rotor-bearing critical speed

[1]These bearings were donated by Torrington through the kindness of W. L. Bowen, whose assistance is gratefully acknowledged.

is predicted to be approximately 12,500 rpm. The end thrust bearing is provided to react the small axial load developed by the opposed test-seal design.

Instrumentation and Data Analysis

The dynamic instrumentation illustrated in Figures 2 and 3 consists, for each seal, of Bently eddy-current motion transducers and five piezo-electric pressure transducers which are distributed both axially and circumferentially along and around the seal. The circumferential "clocking" of the pressure transducers is provided primarily as a matter of convenience, since the transducers are provided exclusively to define the time history of the axial pressure distribution. Since the seal journal is forced to execute a closed circular orbit at constant speed ω within its journal, the steady-state pressure distribution is constant with respect to an observed fixed to the shaft, and the circumferential pressure distribution at time t, $p(z,\theta)$ is definable in terms of either past or future time measurements $p(z,t)$ at a fixed value of θ. The direct extraction of circumferential pressure distributions from pressure time histories also permits the "reconstruction" of a pressure time history at a given circumferential location (e.g., θ=0), despite the fact that the transducers are distributed circumferentially around the seal as illustrated in Figure 3.

The seal reaction forces at a given time, $t = \bar{t}$, are defined by the integrals:

$$R_X(\bar{t}) = -\int_0^{2\pi}\int_0^L p(\theta,z)\,\sin\theta\, R\, d\theta dt = -RL\int_0^{2\pi} \sin\theta\,\bar{p}\,(\theta)\,d\theta$$

$$R_Y(\bar{t}) = -\int_0^{2\pi}\int_0^L p(\theta,z)\,\cos\theta\, R\, d\theta dz = -RL\int_0^{2\pi} \cos\theta\,\bar{p}\,(\theta)\,d\theta \qquad (6)$$

where $\bar{p}$ is the average axial pressure defined by

$$\bar{p}(\theta) = \frac{1}{L}\int_0^L p(\theta,z)dz.$$

The integral of Eq. (6) is evaluated numerically from pressure time histories corresponding to $\theta = 0$ measurements, and denoted $p_1^*(\theta)$. The axial spacing of the pressure transducers has been chosen from Gauss-Legendre quadrature formulas [13] to minimize the error involved in evaluating this integral. The quadrature formula for integration with respect to z is;

$$p(\theta) = \tfrac{1}{2}[A_1 p_1^*(\theta) + A_2 p_2^*(\theta) + A_3 p_3^*(\theta) + A_2 p_4^*(\theta) + A_1 p_5^*(\theta)]$$

where

$$A_1 = 0.23603,\ A_2 = 0.47862,\ \text{and}\ A_3 = 0.56889.$$

Data Analysis Procedure

The dimensional form of Eq. (4) is

$$\begin{bmatrix} M & m \\ -m & M \end{bmatrix} \begin{Bmatrix} \ddot{r}_X \\ \ddot{r}_Y \end{Bmatrix} + \begin{bmatrix} C & c \\ -c & C \end{bmatrix} \begin{Bmatrix} \dot{r}_X \\ \dot{r}_Y \end{Bmatrix} + \begin{bmatrix} K & k \\ -k & K \end{bmatrix} \begin{Bmatrix} r_X \\ r_Y \end{Bmatrix} = - \begin{Bmatrix} R_X \\ R_Y \end{Bmatrix} \tag{7}$$

The nature of the test rig is such that steady synchronous motion of the form

$$r_X = A \cos \omega t \ , \ r_Y = A \sin \omega t \tag{8}$$

results, and for this type of motion, the six coefficients of Eq. (7) can not be separately identified. In fact, only two independent numbers result from the steady-state, harmonic test data ($r_X(t)$, $r_Y(t)$, $R_X(t)$, $R_Y(t)$) which is generated by the test rig for a given axial and circumferential Reynolds number set (R_a,R_c). For the present study, the two numbers chosen for presentation are the radial and circumferential components of the reaction force. From Eqs. (7) and (8), these components may be stated

$$\begin{aligned} R_\theta/A &= \frac{|\bar{r} \times \bar{R}|}{A^2} = k - C\omega - m\omega^2 \\ R_r/A &= \frac{\bar{r} \cdot \bar{R}}{A^2} = M\omega^2 - c\omega - K \ . \end{aligned} \tag{9}$$

TEST RESULTS AND DISCUSSION

Test Results

Static test results for the seals consists of leakage. Dynamic test results are the radial and circumferential force components, (R_r/A, R_θ/A), of Eq. (9) as a function of Reynolds numbers (R_a,R_c). Table 2 contains both static and dynamic test results. With respect to static results, for $\xi = 0.5$, the coefficient

$$C_d = 1 + \xi + 2\sigma$$

of Eq. (1) is approximately -5% in error at the higher R_a range ($R_a \cong 24{,}000$) and +3% in error at the lower R_a range ($R_a \cong 4{,}600$). Hence, leakage is generally well predicted by Eq. (1).

An inspection of the Reynolds number sets of Table 2 demonstrates that R_a is held nominally constant, while R_c is varied, with the result that the Reynolds number pairs (R_a,R_c) are clustered about the nominal axial Reynolds numbers [24,760; 18,850; 9,040; 4.580]. These results were obtained by holding the seal-leakage rate constant while varying the rotational speed ω.

The dashed lines of Figures 4 and 5 connect the test data points of Table 2 for the radial (R_r/A) and tangential force components (R_θ/A) as a function of the circumferential Reynolds number, R_c. The test results reflect both the small changes in R_a about the nominal value $\bar{R}_a$ and the obvious changes in R_c resulting from changes in ω.

Discussion of Radial-Force Component Results

Initial discussions of the test results will deal with results for radial-force components of Figure 4, and the comparison of these results to various theoretical predictions of references [7] and [8]. The experimental and theoretical results of interest are denoted as follows in Figure 4:

------*	Experimental results.
°——°——°	Finite-length solution, reference [8].
Δ——Δ——Δ	Short-seal solution, reference [8].
+——+——+	Short-seal solution, reference [7].
◇——◇——◇	K from reference [8].

The theoretical results of reference [8] would, presumably, provide the best prediction of the radial force component; however, the results of Figures 4(a) through (e) show that: (1) measured radial forces are roughly twice as large as predicted values, and (2) the magnitudes of measured forces tend to increase with increasing R_c, while theoretical predictions show a decreasing magnitude.

As noted in the introduction, short-seal solutions are obtained by neglecting the "pressure-induced" circumferential flow, while including the shear-induced flow. Short-seal solutions yield larger radial force predictions, and, as expected, reduce the discrepancy between theory and experiments of Figure (4). The short-seal solution of reference [8] is developed under less restrictive assumptions than that of reference [7], and agrees better with the test data. The direct stiffness prediction of these two solutions are comparable; however, reference [7] predicts values for M and c that are approximately twice as large as those of reference [8]. The large value for M explains why this solution diverges from both the experimental data and the remaining theoretical solutions with increasing R_c.

In fact, all solutions predict magnitudes for M which are excessive in comparison to either test results or experience with predictions of pumps. An overprediction of M would explain why the theory predicts a reduction in R_θ with increasing R_c, while test results show the opposite. The short-seal theoretical results show that M and c arise from the same momentum terms in the governing equations; hence, if the theory overpredicts M, one would assume that c is comparably overpredicted. If both these terms are eliminated from Eq. (90), only the direct stiffness K remains. This coefficient is illustrated in Figures 4(a) through (e) for the short-seal solution of reference [8].

The coefficient K from the short-seal solution generally behaves the same way as the test results for changes in R_a and R_c, and provides a much better prediction for the radial force component R_θ than the other approaches of Figure 4. However, it underpredicts the test results on the average by about twenty percent.

Discrepancies between theory and experiment illustrated in Figures 4(a) through (e) may be explained as a combination of the following factors:

(a) The theoretical developments are based on a perturbation analysis which assumes that the seal-orbit amplitude A is small compared to the radial clearance C_r, and that second-order terms in A/C_r are negligible. However, for the current apparatus, $A/C_r = 0.25$, and second-order effects may be influencing test results. This may provide part of the explanation for the

seals being stiffer than predicted.

(b) The fundamental bulk-flow model, as presented by the momentum and continuity equations, is, in some sense, deficient. An explanation of this nature is required to explain the apparent major overprediction of the direct added-mass and cross-coupled damping coefficients.

Discussion of Tangential Force Components

Theoretical results for the cross-coupled, added-mass coefficient m typically indicate a negligible contribution to the tangential force component, i.e.,

$$R_\theta/A \cong k - C\omega \ .$$

Further, in the test apparatus, the shaft rotates in a clockwise sense and the tangential force would be defined by

$$R_\theta/A \cong -k + C\omega \ . \tag{10}$$

A comparison of the test results with the finite-length solution predictions in Figures 5(a) through (e) shows generally good agreement. If the test results were curvefitted by a linear curve of the form predicted by Eq. (10), one would reach the following conclusions:

(a) The cross-coupled coefficient k is smaller than predicted, and the difference between theory and experiment increases with increasing R_a. This conclusion is supported by noting that measured values for R_θ/A are smaller than predicted at low values of R_c.

(b) The damping coefficient C is slightly smaller than predicted. The generally steeper slopes for the experimental data curve supports this conclusion.

The finite-length solution of [8] generally provides a better correlation with experimental data than either of the short-seal solutions. All of these solutions include the influence of "swirl." Specifically, in contrast to typical hydrodynamic-bearing analyses in which the fluid is assumed to have an average circumferential velocity of $R\omega/2$, the acceleration of a fluid particle due to shear forces is accounted for. For short-seals with high axial fluid velocities, this means that a fluid particle may exit the seal without acquiring a substantial tangential velocity. Since the test rig of Figure 2 provides negligible pre-rotation of fluid entering the seal, the theory assumes that the inlet circumferential velocity is zero. Predictions of k are substantially reduced by including the influence of swirl; hence, test results of Figure 5 provide an additional verification of the influence of swirl.

SUMMARY AND CONCLUSIONS

The test results presented support the following general conclusions:

(a) Leakage is reasonably well predicted by Yamada's model.

(b) The circumferential force, which primarily represents the direct damping coefficient C and cross-coupled stiffness coefficient k, is adequately predicted by the finite-length theory of reference [8].

(c) The radial force is substantially underpredicted (40 to 50%) by the finite-length theory. The direct, added-mass coefficient M appears to be much smaller than predicted by theory. By inference, the cross-coupled damping coefficient c is probably also much smaller than predicted.

(d) The direct stiffness K from the short-seal solution of reference [8] has the

same form as the measured radial force component but is approximately 20% less than measured values.

A conclusive explanation for the discrepancies between the theory and experimental results for the radial force component is not possible; however, it may result from either (a) nonlinearities due to the size of the seal orbits relative to the radial clearance, or (b) basic inadequacies in the bulk-flow model.

On the basis of the present results, the following reduced model for seal reaction forces is recommended for modelling seals in rotordynamics analysis of pumps:

$$-\begin{Bmatrix} R_X \\ R_Y \end{Bmatrix} = \begin{bmatrix} K & k \\ -k & K \end{bmatrix} \begin{Bmatrix} X \\ Y \end{Bmatrix} + \begin{bmatrix} C & 0 \\ 0 & C \end{bmatrix} \begin{Bmatrix} \dot{X} \\ \dot{Y} \end{Bmatrix} .$$

Note that the added-mass and cross-coupled coefficients have been discarded. The coefficients of k and C are adequately predicted by the finite-length solution of reference [8]. The best prediction for K is provided by the short-seal solution of reference [8]; however, this prediction is approximately 20% lower than test results.

REFERENCES

1. Black, H. F., "effects of Hydraulic Forces in Annular Pressure Seals on the Vibrations of Centrifugal Pump Rotors," J. M. Eng. Sci., vol. 11, No. 2, pp. 206-213, 1969.

2. Black, H. F. and Jensen, D. N., "Dynamic Hybrid Properties of Annular pressure Seals," Proc. J. Mech. Engin., vol. 184, pp. 92-100, 1970.

3. Black, H. F. and Jensen, D. N., "Effects of High Pressure Ring Seals on Pump Rotor Vibrations," ASME Paper No. 71-WA/FF-38, 1971.

4. Black, H. F., Allaire, P.E., and L. E. Barrett, "The Effect of Inlet Flow Swirl on the Dynamic Coefficients of High-Pressure Annular Clearance Seals, "Ninth International Conference in Fluid Sealing, BHRA Fluids Engineering, Leeuwenhorst, The Netherlands, April 1981.

5. Childs, D. W., "The Space Shuttle Main Engine High-Pressure Fuel Turbopump Rotordynamic Instability Problem," ASME Transactions for Power, pp. 48-57, January 1978.

6. Yamada, Y., "Resistance of Flow through Annulus with an Inner Totating Cylinder, "Bul. J.S.M.E., vol. 5, No. 18, pp. 302-310, 1962.

7. Childs, C. W., "Dynamic Analysis of Turbulent Annular Seals Based on Hirs' Lubrication Equation," accepted for publication, ASME Trans., J. of Lubrication Technology.

8. Childs, D. W., "Finite-Length Solution for Turbulent Annular Seals," Accepted for publications, ASME Trans., J. of Lubrication Technology.

9. Hirs, G. G., "A Bulk-Flow Theory for Turbulence in Lubricant Films," ASME J. Lubrication Technology, pp. 137-146, April 1973.

10. Black, H. F., "Empirical Treatment of Hydrodynamic Journal Bearing Performance in the Superlaminer Regime," J. Mech. Engine. Sci., vol. 12, no. 2, pp. 116-122, 1970.

11. Black, H. F. and Cochrane, E. A., "Leakage and Hybrid Bearing Properties of Serrated Seals in Centrifugal Pumps," Paper G5, 6th International Conference on Fluid Sealing, February 27-March 2, 1973, Munich German Federal Republic.

12. Bowen, W. L. and Bhateje, R., "The Hollow Roller Bearing," ASME Paper No. 79-Lub-15, ASME-ASLE Lubrication Conference, Dayton, Ohio; 16-18 October 1979.

13. Fröberg, Introduction to Numerical Analysis, Second Edition, Addison Wesley, 1969.

TABLE 1. - PRIOR DYNAMIC SEAL TESTS

REF.	R_a	R_c	L/D	$(C_r/R) \times 10^3$	Seal type	Cited Results
[2]	[6,000, 14,000]	[0, 3,500]	.25 , .5, 1.	10.5 , 12.9	plain	a, b, c
[3]	[3,000, 20,000]	[0, 6,000]	.5, 1.	7.23, 10.3	plain	d, e
[10]	10,000	[0, 8,000]	1.	10.7	plain	f
[11]	[3,000, 12,000]	[0, 6,000]	.232, .5, 1.	7.1	Serrated	d

a. Static force-deflection curves for $0 \leq \varepsilon \leq 0.8$.

b. Resultant stiffness F_s/r for centered position and $\omega = 0$.

c. Rotordynamic modelling to correlate with test data on the direct damping coefficient $\bar{c}$.

d. Receptance magnitudes for centered position.

e. Rotordynamic modelling to correlate with synchronous test results. Correlation includes amplitude, phase, critical speed, and onset speed of instability.

f. Receptance magnitude and phase at centered position.

TABLE 2. - EXPERIMENTAL RESULTS FOR A CONSTANT-CLEARANCE SEAL, L = R = 2 in. (5.08 cm), C_r = 0.020 in. (0.508 mm)

	R_a	R_c	ΔP(psi)	Leakage (gpm)	ω(rpm)	R_r/A(lbs/in)	R_θ/A(lbs/in)
1	24,580	3,160	113.	62.0	1,149.	-13,950.	3,507.
2	23,550	5,800	99.	58.5	2,105.	-13,190	6,800.
3	26,780	7,950	121.	66.51	1,885.	-16,150.	11,870.
4	25,330	8,840	113.	62.9	3,209.	-15,500.	12,790.
5	23,545	10,360	106.	58.5	3,762.	-15,090.	16,540.
6	18,140	2,878	62.0	45.1	1,054.	- 7,886.	2,344.
7	19,990	5,860	65.0	47.1	2,178.	- 8,507.	5,821.
8	18,730	8,260	65.0	46.5	3,000.	- 8,790.	9,250.
9	18,560	10,660	71.0	46.1	3,871.	-11,120.	12,750.
10	13,330	3,040	34.0	33.1	1,103.	- 4,125.	2,503.
11	13,510	6,360	36.0	33.6	2,308.	- 5,014.	4,360.
12	13,060	8,880	35.0	32.4	3,226.	- 6,030.	&,802.
13	13,610	9,860	41.0	33.8	3,582.	- 7,430.	9,170.
14	9,010	2,920	17.0	22.4	1,060.	- 2,276.	1,597.
15	8,850	5,840	19.0	22.0	2,120.	- 2,240.	3,210.
16	9,260	8,610	21.0	23.0	3,125.	- 2,095.	5,715.
17	4,750	2,700	5.0	11.8	980.4	- 670.	812.
18	4,410	4,920	3.0	11.0	1,786.	- 645.	1,475.
19	4,750	8,220	4.0	11.8	2,985.	- 578.	2,763.
20	4,410	10,630	5.0	11.0	3,859.	- 417.	3,492.

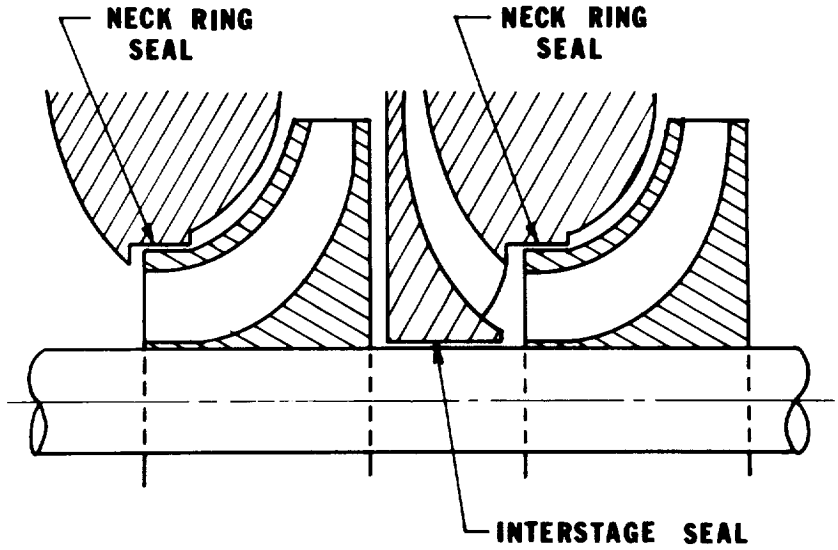

Figure 1. - Neck-ring and interstage seals for pumps.

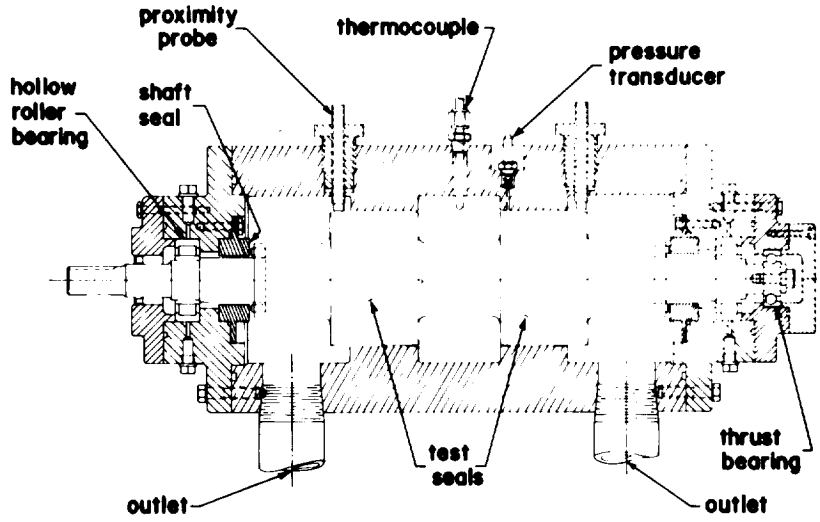

Figure 2. - Test-section layout.

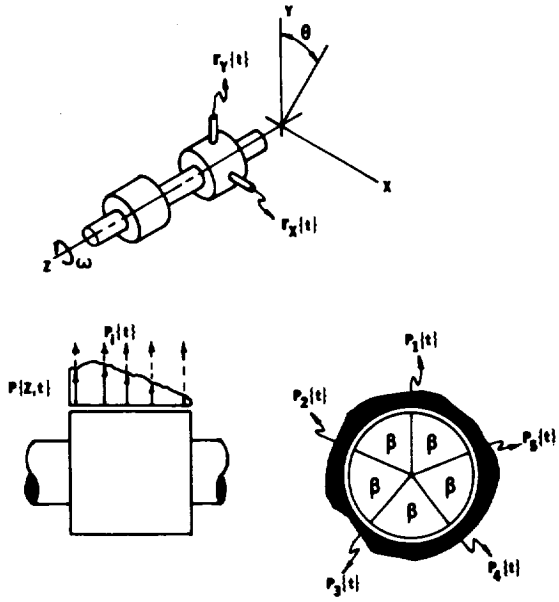

Figure 3. - Instrumentation.

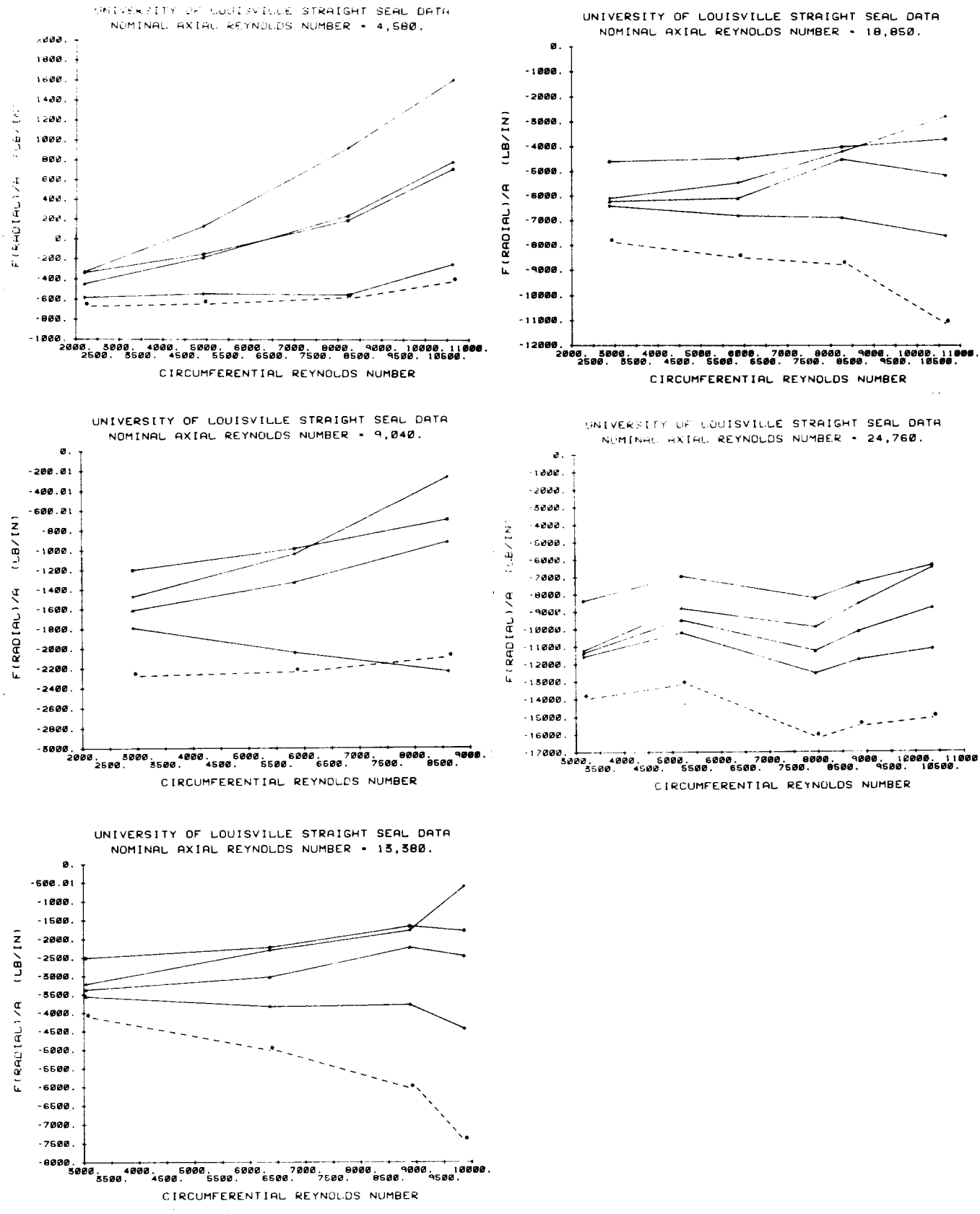

Figure 4. - Seal radial-force component versus axial and circumferential Reynolds numbers.

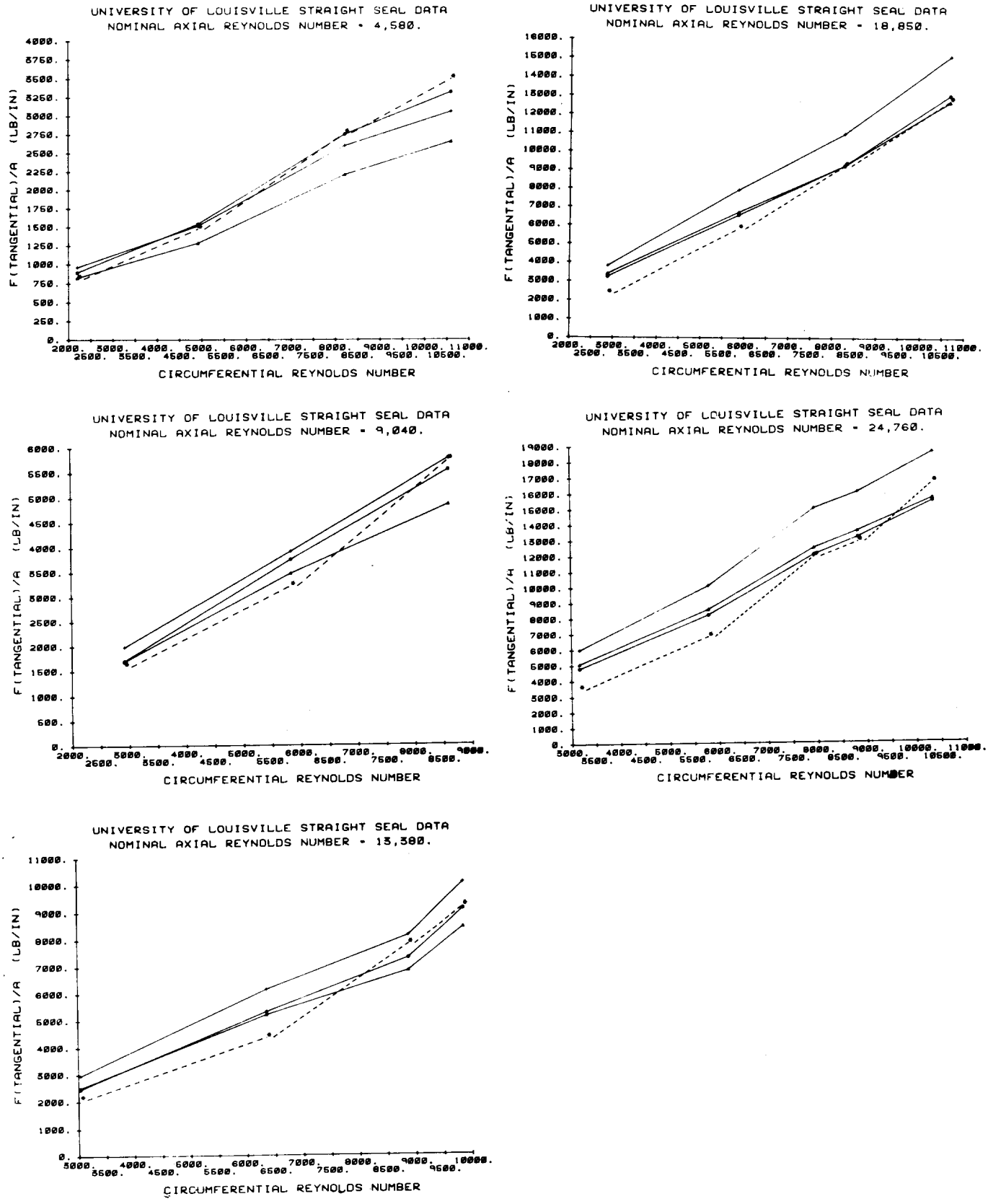

Figure 5. - Seal tangential-force component versus axial and circumferential Reynolds numbers.